Article

Cell Reports

Dynamic Metabolomics Reveals that Insulin Primes the Adipocyte for Glucose Metabolism

Graphical Abstract

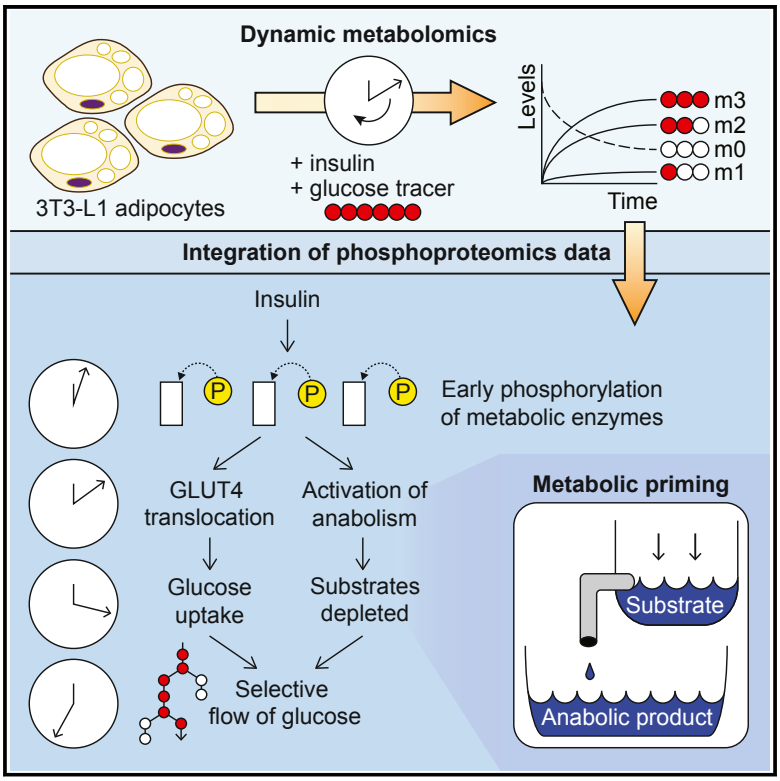

Authors

James R. Krycer, Katsuyuki Yugi, Akiyoshi Hirayama, ..., Tomoyoshi Soga, Shinya Kuroda, David E. James

Correspondence

skuroda@bs.s.u-tokyo.ac.jp (S.K.), david.james@sydney.edu.au (D.E.J.)

In Brief

Krycer et al. explore how insulin regulates adipocyte metabolism. It is widely held that energy storage (anabolism) occurs as a substrate accumulates. However, using dynamic tracer metabolomics and overlaying phosphoproteomics data, they find that insulin signaling triggers anabolism before substrates accumulate, creating a "demand-driven" system to prime adipocytes for glucose metabolism.

Highlights

- Dynamic ^{13}C-tracer metabolomics shows insulin rapidly alters adipocyte metabolism
- Glucose flow favors specific pathways, such as pyruvate anaplerosis
- Besides glucose uptake, insulin triggers anabolism before substrates accumulate
- Insulin-dependent phosphorylation primes adipocytes for glucose metabolism

Krycer et al., 2017, Cell Reports *21*, 3536–3547
December 19, 2017
https://doi.org/10.1016/j.celrep.2017.11.085

CellPress

OPEN ACCESS
CellPress

Cell Reports
Article

Dynamic Metabolomics Reveals that Insulin Primes the Adipocyte for Glucose Metabolism

James R. Krycer,[1,2,19] Katsuyuki Yugi,[6,7,10,11,19] Akiyoshi Hirayama,[11,12] Daniel J. Fazakerley,[1,2] Lake-Ee Quek,[2,3] Richard Scalzo,[13] Satoshi Ohno,[6] Mark P. Hodson,[14,15,16] Satsuki Ikeda,[11] Futaba Shoji,[11] Kumi Suzuki,[11] Westa Domanova,[2,4] Benjamin L. Parker,[1,2] Marin E. Nelson,[1,2] Sean J. Humphrey,[1,2] Nigel Turner,[17] Kyle L. Hoehn,[18] Gregory J. Cooney,[2,5] Tomoyoshi Soga,[11,12] Shinya Kuroda,[6,8,9,20,*] and David E. James[1,2,5,20,21,*]

[1]School of Life and Environmental Sciences, University of Sydney, Sydney, NSW 2006, Australia
[2]Charles Perkins Centre, University of Sydney, Sydney, NSW 2006, Australia
[3]School of Mathematics and Statistics, The University of Sydney, Sydney NSW 2006, Australia
[4]School of Physics, University of Sydney, Sydney, NSW 2006, Australia
[5]Sydney Medical School, University of Sydney, Sydney, NSW 2006, Australia
[6]Department of Biological Sciences, Graduate School of Science, University of Tokyo, Hongo 7-3-1, Bunkyo-ku, Tokyo 113-0033, Japan
[7]YCI Laboratory for Trans-Omics, Young Chief Investigator Program, RIKEN Center for Integrative Medical Sciences, 1-7-22 Suehiro-cho, Tsurumi-ku, Yokohama, Kanagawa 230-0045, Japan
[8]Department of Computational Biology and Medical Sciences, Graduate School of Frontier Sciences, University of Tokyo, 5-1-5 Kashiwanoha, Kashiwa, Chiba 277-8562, Japan
[9]CREST, Japan Science and Technology Agency, Bunkyo-ku, Tokyo 113-0033, Japan
[10]PRESTO, Japan Science and Technology Agency, 1-7-22 Suehiro-cho, Tsurumi-ku, Yokohama, Kanagawa 230-0045, Japan
[11]Institute for Advanced Biosciences, Keio University, Tsuruoka, Yamagata 997-0052, Japan
[12]AMED-CREST, AMED, 1-7-1 Otemachi, Chiyoda-Ku, Tokyo 100-0004, Japan
[13]Centre for Translational Data Science, University of Sydney, Sydney, NSW 2006, Australia
[14]Metabolomics Australia Queensland Node, Australian Institute for Bioengineering and Nanotechnology, University of Queensland, Brisbane, QLD 4072, Australia
[15]School of Pharmacy, Faculty of Health and Behavioural Sciences, University of Queensland, Brisbane, QLD 4072, Australia
[16]Metabolomics Research Laboratory, Victor Chang Innovation Centre, Victor Chang Cardiac Research Institute, Darlinghurst, NSW 2010, Australia
[17]School of Medical Sciences, University of New South Wales, Sydney, NSW 2052, Australia
[18]School of Biotechnology and Biomolecular Sciences, University of New South Wales, Sydney, NSW 2052, Australia
[19]These authors contributed equally
[20]Senior author
[21]Lead Contact
*Correspondence: skuroda@bs.s.u-tokyo.ac.jp (S.K.), david.james@sydney.edu.au (D.E.J.)
https://doi.org/10.1016/j.celrep.2017.11.085

SUMMARY

Insulin triggers an extensive signaling cascade to coordinate adipocyte glucose metabolism. It is considered that the major role of insulin is to provide anabolic substrates by activating GLUT4-dependent glucose uptake. However, insulin stimulates phosphorylation of many metabolic proteins. To examine the implications of this on glucose metabolism, we performed dynamic tracer metabolomics in cultured adipocytes treated with insulin. Temporal analysis of metabolite concentrations and tracer labeling revealed rapid and distinct changes in glucose metabolism, favoring specific glycolytic branch points and pyruvate anaplerosis. Integrating dynamic metabolomics and phosphoproteomics data revealed that insulin-dependent phosphorylation of anabolic enzymes occurred prior to substrate accumulation. Indeed, glycogen synthesis was activated independently of glucose supply. We refer to this phenomenon as metabolic priming, whereby insulin signaling creates a demand-driven system to "pull" glucose into specific anabolic pathways. This complements the supply-driven regulation of anabolism by substrate accumulation and highlights an additional role for insulin action in adipocyte glucose metabolism.

INTRODUCTION

Adipose tissue is essential for whole-body glucose homeostasis, exemplified by the detrimental metabolic consequences of lipodystrophies and the beneficial effects of thiazolidinediones, which enhance adipocyte cell numbers (Rosen and Spiegelman, 2014). While initially considered simply a storage depot for nutrients consumed during a meal, recent studies highlight additional functions for adipose tissue in metabolic homeostasis such as the release of adipokines. Although adipose tissue only contributes ~5% to whole-body glucose disposal following a meal (DeFronzo and Tripathy, 2009), reduced adipocyte glucose uptake is one of the earliest defects in insulin resistance (Garvey and Kolterman, 1988; Kraegen et al., 1991; Turner et al., 2013). Furthermore, adipocyte-specific knockout of the insulin-responsive glucose transporter, GLUT4, causes whole-body insulin

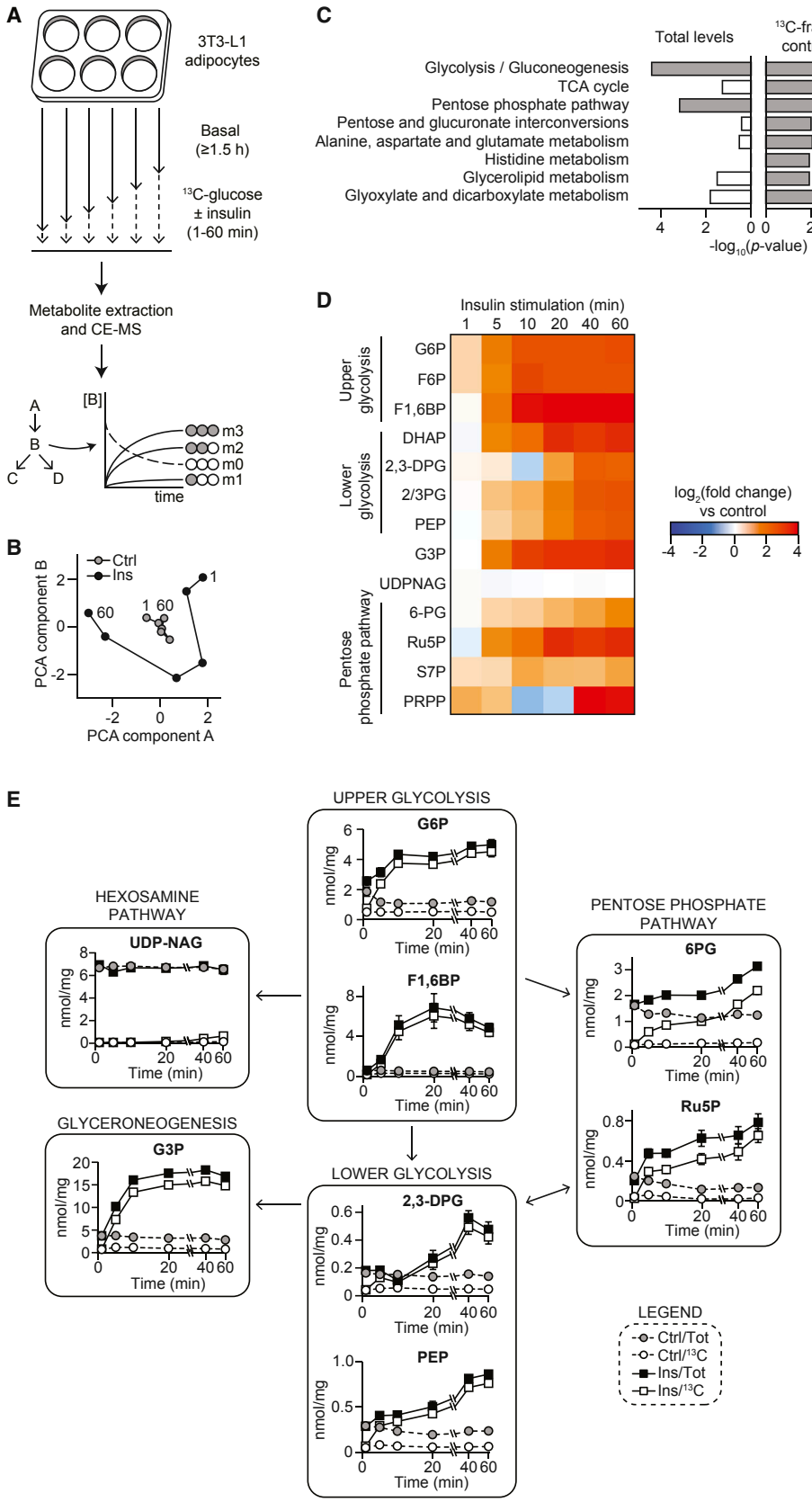

(legend on next page)

resistance (Abel et al., 2001), whereas adipose-specific GLUT4 overexpression improves glucose homeostasis (Herman et al., 2012). This demonstrates that the way in which adipocytes metabolize and store glucose is central to whole-body glucose homeostasis. Thus, it is of great interest to better understand how glucose metabolism is regulated in the adipocyte.

Cellular metabolism is acutely regulated at the metabolite level via the concentrations of substrates and allosteric regulators (Hackett et al., 2016). For instance, glycogen synthesis increases with a rise in intracellular glucose levels and the allosteric regulator of glycogen synthase, glucose 6-phosphate (Bouskila et al., 2010). Likewise, malonyl-coenzyme A (malonyl-CoA) blocks beta-oxidation to shift the balance toward lipogenesis when glucose availability increases (McGarry et al., 1978). Furthermore, the balance between anabolism and catabolism is finely tuned by the energy charge ratio, which is driven by changes in ATP, ADP, and AMP levels (Atkinson, 1968). This serves to maintain homeostasis by ensuring that energy storage occurs when substrates are in excess of energy requirements.

Control at the metabolite level is complemented by the post-translational modification of proteins via hormonal regulation. For instance, glucose metabolism in adipocytes is particularly responsive to insulin, which enhances glucose uptake, oxidation, and storage into lipid and glycogen (Foley et al., 1980; Katz et al., 1966; Katz and Rognstad, 1966; Rodbell, 1964; Winegrad and Renold, 1958a, 1958b). This insulin signal is transmitted by a signal transduction cascade of kinase-mediated protein phosphorylation targeting key proteins such as those regulating the translocation of GLUT4 to the plasma membrane (Stöckli et al., 2011). Glucose transport is generally considered to be the major regulatory step in the metabolic response to insulin in adipocytes (Bryant et al., 2002). However, we recently reported widespread phosphorylation changes in the adipocyte in response to insulin, including numerous metabolic proteins (Humphrey et al., 2013), and it is unclear how these changes influence the dynamics of glucose metabolism upon insulin exposure.

In this study, we assessed the acute response of the adipocyte metabolome to insulin exposure and integrated this with changes in the insulin-regulated phosphoproteome to understand the role of phosphorylation in glucose metabolism. In contrast to traditional steady-state experiments, we applied a dynamic approach to tracer metabolomics. We found that within minutes, insulin rapidly stimulated the transport and incorporation of glucose into central carbon metabolites. Glucose metabolism was highly selective, favoring specific glycolytic branch points and was bifurcated between the tricarboxylic acid (TCA) cycle and pyruvate anaplerosis (via pyruvate carboxylase). While glucose uptake was a major driver of this metabolomic-wide variation, a transomic analysis (Yugi et al., 2014, 2016) revealed insulin-stimulated phosphorylation played a role beyond glucose uptake. In general, phosphorylation occurred early before glucose transport was maximal, activating key anabolic pathways to potentially coerce glucose into specific metabolic pathways. We propose that this demand-driven "pull" system complements the regulation of anabolism by subsequent substrate accumulation "push" mechanisms. This reveals an additional role for the regulation of glucose metabolism by insulin beyond glucose uptake.

RESULTS

Insulin Induces Rapid and Selective Changes in Metabolism

To examine the dynamic metabolic response to insulin, we conducted an acute metabolomics analysis of 3T3-L1 adipocytes treated with insulin for up to 1 hr (Figure 1A; additional details in the Experimental Procedures). This was performed in the presence of [U-^{13}C]-labeled glucose to track the metabolism of glucose-derived carbon atoms. Polar metabolites were measured by targeted capillary electrophoresis-coupled mass spectrometry (CE-MS), resulting in the quantification of 203 metabolites (Table S1).

We examined the insulin response using a principal-component analysis (PCA) across the metabolite domain (Figure 1B). This revealed dynamic regulation of the metabolome, exhibiting two distinct phases occurring between 1–20 min and 20–60 min. In contrast, little change was observed in unstimulated cells. Specifically, the total levels of 66 metabolites changed in response to insulin, and 57 metabolites showed an altered ^{13}C-labeled fractional contribution (FC) (Table S2). An enrichment analysis revealed an overrepresentation of the major

Figure 1. Insulin Stimulates Rapid yet Selective Changes in Central Carbon Metabolism

(A) Experimental outline for the dynamic metabolomics experiment. 3T3-L1 adipocytes were serum starved and then labeled with [U-^{13}C]-glucose tracer, with or without insulin, in a reverse-time-course format. Metabolite isotopologue concentrations were quantified by capillary electrophoresis-coupled mass spectrometry (CE-MS). Additional details on the experimental design are provided in the Experimental Procedures.

(B–E) 3T3-L1 adipocytes were treated with (Ins) or without (control, Ctrl) 100 nM insulin for the indicated time points, as described in Figure 1A. Data were obtained from n = 3 separate experiments.

(B) PCA of total metabolite levels from Ins- and Ctrl-treated cells, across the metabolite domain. This analysis reduced the dimension of the metabolome and treated time points as separate samples. The lines connect adjacent time points (1, 5, 10, 20, 40, and 60 min), with the first and last time points indicated on the plot. The contribution of each metabolite to components A and B is depicted in Figure S1A.

(C) Enrichment analysis of metabolites whose total levels and ^{13}C-labeled fractional contribution changed between control (Ctrl) and insulin (Ins)-treated cells. Uncorrected p values are depicted, with significant pathways (false discovery rate [FDR] < 0.1) indicated in gray. Results of the complete analysis can be found in Table S2.

(D) Changes in total levels of selected metabolites presented as the mean fold-change between insulin-treated and control-treated cells.

(E) Total and ^{13}C-labeled levels for selected metabolites. Data are presented as mean ± SEM.

2,3-DPG, 2,3-diphosphoglycerate; 2/3-DPG, 2- and 3-phosphoglycerate; 6-PG, 6-phosphogluconate; DHAP, dihydroxyacetone phosphate; F1,6BP, fructose 1,6-bisphosphate; F6P, fructose 6-phosphate; G3P, glycerol 3-phosphate; G6P, glucose 6-phosphate; PEP, phosphoenolpyruvate; PRPP, phosphoribosyl pyrophosphate; Ru5P, ribulose 5-phosphate; S7P, sedoheptulose 7-phosphate; TCA, tricarboxylic acid; UDPNAG, uridine diphosphate N-acetylglucosamine.

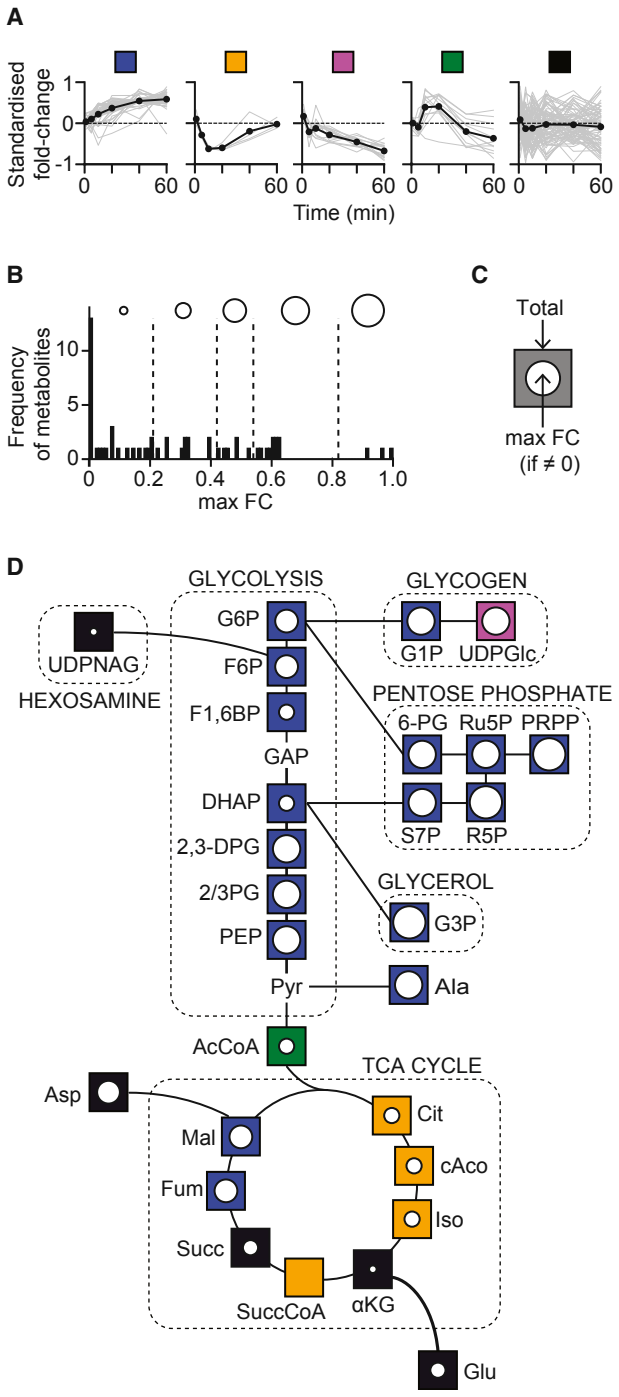

Figure 2. Clustering Analyses Reveal that Insulin Stimulates Distinct Temporal Patterns in Central Carbon Metabolism

3T3-L1 adipocytes were serum starved and treated with (Ins) or without (control [Ctrl]) 100 nM insulin for the indicated time points, as described in Figure 1A. Data were obtained from n = 3 separate experiments.

(A and B) Metabolites were clustered by the insulin-responsive changes in total metabolite levels (A) and maximum ^{13}C-labeled fractional contribution (max FC) (B). Details of the analytical procedures are described in Experimental Procedures, and results of the complete analysis can be found in Table S3.

(C and D) Each metabolite was represented by the symbols depicted above each group in (A) (colored squares) and (B) (open circles of different sizes), as shown in (C). This was used to construct the graphical representation of central carbon metabolism in (D).

2,3-DPG, 2,3-diphosphoglycerate; 2/3-DPG, 2- and 3-phosphoglycerate; 6-PG, 6-phosphogluconate; Ala, alanine; Asp, aspartate; AcCoA, acetyl-CoA; cAco, *cis*-aconitate; Cit, citrate; DHAP, dihydroxyacetone phosphate; F1,6BP, fructose 1,6-bisphosphate; F6P, fructose 6-phosphate; Fum, fumarate; G1P, glucose 1-phosphate; G3P, glycerol 3-phosphate; G6P, glucose 6-phosphate; GAP, glyceraldehyde 3-phosphate; Glu, glutamate; Iso, isocitrate; Mal, malate; PEP, phosphoenolpyruvate; PRPP, Phosphoribosyl pyrophosphate; Pyr, pyruvate; Ru5P, ribulose 5-phosphate; S7P, sedoheptulose 7-phosphate; Succ, succinate; SuccCoA, succinyl-CoA; TCA, tricarboxylic acid; UDPGlc, uridine diphosphate glucose; UDPNAG, uridine diphosphate N-acetylglucosamine; αKG, α-ketoglutarate.

pathways involved in central carbon metabolism (Figure 1C; Table S2).

Insulin rapidly increased metabolite concentrations in upper glycolysis (glucose 6-phosphate to fructose 1,6-bisphosphate), reaching a new steady state by 10 min (Figure 1D). At this time point, the insulin/control ratio for 2,3-diphosphoglycerate decreased below 1 (Figure 1D), indicating that this "crossover" point corresponds to a potential site of regulation (Holmes, 1959; Moreno-Sánchez et al., 2008). This is reflected by lower glycolysis, where metabolites took much longer (~40 min) to reach an equilibrium (Figure 1E). Thus, these acute time points provided the temporal resolution to distinguish how the two glycolytic phases responded differently to insulin.

Next, we compared pathways branching from upper glycolysis to determine whether there was selectivity in glucose partitioning. Metabolites in the oxidative pentose phosphate pathway (PPP) increased rapidly, while there was little change in the hexosamine pathway (Figures 1D and 1E). This was reflected by greater ^{13}C-enrichment in PPP intermediates compared to the hexosamine pathway (Figure 1E). This suggests that glucose does not simply distribute throughout all side branches of glycolysis; rather, its metabolism is directed toward specific pathways.

Insulin Rapidly Bifurcates Glucose Flow into the TCA Cycle and Pyruvate Anaplerosis

We next sought to empirically define bona fide routes of metabolic flow within the adipocyte. We reasoned that adjacent metabolites that responded to insulin with similar kinetic and directional change likely constituted a route of metabolic flow. Using unbiased clustering analyses (Table S3; detailed in the Experimental Procedures and the Supplemental Experimental Procedures), we segregated metabolites based on insulin-dependent changes in total levels over time (Figure 2A) and maximum FC (Figure 2B). We compared these two parameters visually (Figure 2C) to determine how insulin changed the total levels of each metabolite and how ^{13}C-glucose (FC) contributed to these changes. Mapping this to adjacent metabolites in central carbon metabolism revealed several distinct patterns (Figure 2D).

Specifically, the majority of glycolysis clustered together, with total levels increasing over time and generally large FCs implying glucose is responsible for these changes (Figure 2D). In contrast, the TCA cycle was heterogeneous; malate and fumarate responded similarly to glycolytic metabolites, while the remaining metabolites displayed lower FCs and occupied different total-level clusters (Figure 2D). Specifically, the total levels of malate

and fumarate increased monotonically (without a change in direction) in response to insulin, whereas the metabolites from citrate to succinate initially decreased before rising (Figure 3A). Furthermore, malate and fumarate had higher FCs than the other TCA cycle metabolites.

A possible explanation for these differences between the TCA cycle metabolites came from the analysis of the individual isotopologues. For each time point, we examined the levels of each individual isotopomer as a proportion of the total metabolite levels, depicted visually using heatmaps (Figure 3A, right panel for each metabolite). For instance, the m3 isotopologue was dominant for malate and fumarate (Figure 3A), as well as for aspartate (Figure S2C), which serves as a surrogate for the labeling of oxaloacetate since the media did not contain aspartate. In contrast, the ^{13}C-labeling of succinate consisted predominantly of m2 and m4 isotopologues (Figure 3A). Together, this is indicative of pyruvate anaplerosis via pyruvate carboxylase (Buescher et al., 2015), which has been reported by steady-state labeling to be the major source of reduced nicotinamide adenine dinucleotide phosphate (NADPH) production within adipocytes (Liu et al., 2016). Remarkably, these patterns were evident within 5 min of insulin stimulation, rapidly depleting the unlabeled fraction of malate and fumarate (m0 at 60 min = 0.16 ± 0.01 and 0.18 ± 0.01, respectively), implicating exogenous glucose as the main contributor to this pathway in insulin-stimulated cells.

Glucose Transport Explains a Majority of the Metabolomic Variation in Response to Insulin

Next, we used PCA to identify potential drivers of the temporal metabolic response to insulin. Central carbon metabolites could be divided into distinct clusters with two principal components (Figure 3B), including the separation of malate and fumarate from other TCA cycle metabolites. Component 1 (53% variance) increased in a generally monotonic fashion and component 2 (30% variance) exhibited a biphasic response (Figure 3C). Interestingly, component 2 resembled the kinetics of the energy charge ratio (Figure 3D). The influence of the energy charge ratio is suggested by the global behavior of the insulin-stimulated metabolome (Figure 1B), whereby the first 20 min were driven by component B, which was characterized by marked increases in singly phosphorylated nucleotides (AMP, cytidine monophosphate [CMP], inosine monophosphate [IMP], and uridine monophosphate [UMP]) (Figure S1A).

Since component 1 monotonically increased like glucose transport (Figure 4A, top right), we next assessed how much temporal variation in the metabolome could be explained by glucose transport and energy charge ratio as components. Performing a linear regression, we found that glucose transport and the energy charge ratio could respectively explain 48% and 29% of the variation seen in the metabolome in response to insulin. This concurs with the classic notion that glucose transport poses a major insulin-regulated barrier to glucose metabolism in adipocytes (Bryant et al., 2002), supported here by the total metabolite levels of upper glycolytic intermediates rising on a timescale (Figures 1D and E) similar to glucose uptake (Figure 4A, top right) and being predominantly ^{13}C-labeled in response to insulin (Figures 1E and S1B). It is likely that the remainder of the variation (23%) is explained by allosteric interactions (independent of energy charge) or by acute post-translational modification of metabolic proteins such as phosphorylation.

Kinetics of Insulin-Regulated Protein Phosphorylation versus Metabolism

Next, we sought to determine the potential role of insulin signaling in adipocyte metabolism beyond augmenting glucose uptake. To do this, we utilized our previously published phosphoproteomics dataset (Humphrey et al., 2013), whereby 3T3-L1 adipocytes were treated with insulin over an acute time course (0–60 min). This included rapid time points (e.g., 15, 30, and 60 s) to provide the temporal resolution to segregate the activation of key kinases by using the phosphorylation of their substrates as a surrogate for kinase activity (Domanova et al., 2016). This analysis revealed that the Ser/Thr kinase Akt/protein kinase B (PKB) is activated before S6K kinase, while protein kinase A (PKA) is rapidly deactivated (Figure 4A). Importantly, the dynamics and direction of kinase activity translated to adipocyte function; for instance, insulin rapidly increased glucose transport, an Akt-driven process, whereas we observed a more gradual increase in protein synthesis, which is S6K driven (Figure 4A). This corroborates what has been observed previously in rat adipocytes (Marshall, 1989). In contrast, insulin quickly diminished lipolysis, which is PKA driven (Figure 4A). Therefore, insulin drives the coordinated regulation between kinase activity and biological processes within the cell.

We hypothesized that this temporal cascade in protein phosphorylation may play a similar role in directing insulin-stimulated glucose metabolism (Figure 4B). Teleologically, this would ensure the accumulation of sufficient carbon atoms, energy, and redox potential before the cell invests in expensive processes such as lipogenesis. To test this, we initially overlayed the phosphoproteomic and metabolomics data. Because we were interested in how insulin signaling influenced the metabolism of glucose over time, we considered the ^{13}C-labeled pool for each metabolite. Adopting our previous approach (Yugi et al., 2014), we identified enzymes whose substrates or products changed significantly in response to insulin. For enzymes with insulin-responsive phosphosites (Humphrey et al., 2013), we compared the half-time ($t_{1/2}$) for the change in metabolite (substrate or product) and phosphorylation. We expected a linear correlation whereby, for instance, a late phosphorylation event would be linked to a late change in metabolite levels (Figure 4C). However, insulin-dependent changes in phosphorylation occurred significantly earlier than changes in their metabolites (Figure 4D). Indeed, most phosphorylation events occurred within 10 min, prior to achieving maximal glucose transport (Figure 4A) and ^{13}C-enrichment of early glycolytic metabolites (Figure 1E).

To understand how this influences glucose metabolism, we mapped the phosphorylation sites onto enzymes in central carbon metabolism (Figure 5), where the majority of insulin-responsive changes in ^{13}C-labeling were found (Figure 1C). Most phosphorylation events occurred before the metabolism of glucose (Figure 5), corroborating the correlation plot (Figure 4D). In particular, enzymes involved in anabolism (glycogen and fatty acid synthesis) were substantially phosphorylated within 5 min, before the accumulation of intracellular substrates. This suggests that phosphorylation may either play a passive role in

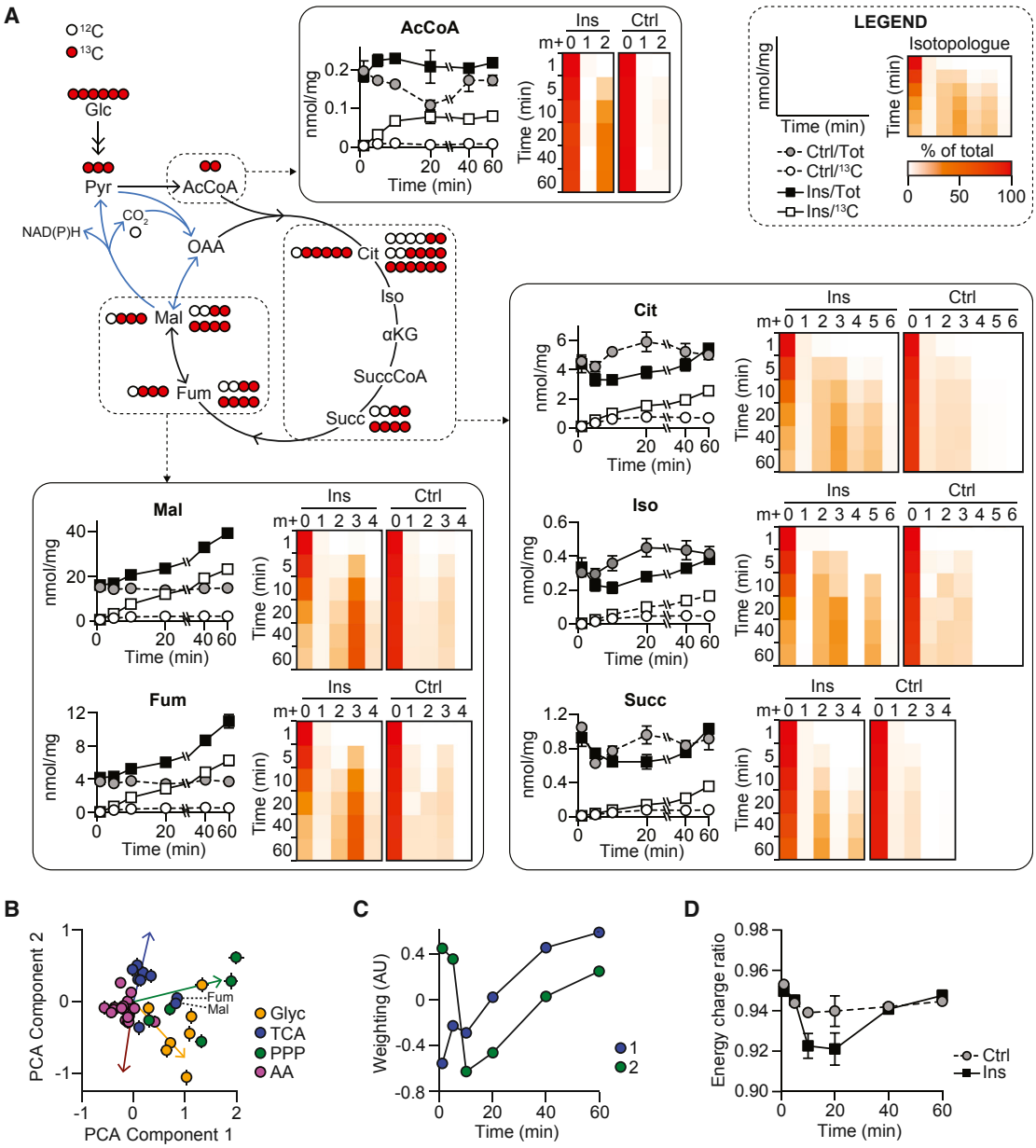

Figure 3. Glucose Tracing Reveals that Insulin Rapidly Bifurcates Glucose Flow between the TCA Cycle and Pyruvate Anaplerosis

3T3-L1 adipocytes were serum starved and treated with (Ins) or without (control [Ctrl]) 100 nM insulin for the indicated time-points, as described in Figure 1A. Data obtained from n = 3 separate experiments.

(A) For each of the selected metabolites, the left panel depicts total and ^{13}C-labeled levels (presented as mean ± SEM). The right panel depicts the mean proportion of each isotopologue compared to the total levels for that treatment and time point.

(B) PCA of the difference in total metabolite levels between insulin-treated and control cells across the time domain. This analysis treated individual metabolites as separate samples and reduced the dimension of time courses to summarize regularities in time-course behavior across the metabolome. Selected metabolites from central carbon metabolism are shown, with x and y error bars depicting SEM. The arrows are subjective labels to highlight the general spread of metabolites from each respective pathway.

(C) The contribution of each time point to components 1 and 2 in Figure 3B.

(D) Energy charge ratio, calculated as (ATP + ½*ADP)/(ATP + ADP + AMP), for insulin-treated and control cells. Data are presented as mean ± SEM.

AA, amino acids; AcCoA, acetyl-CoA; Cit, citrate; Fum, fumarate; Glc, glucose; Glyc, glycolysis; Iso, isocitrate; Mal, malate; OAA, oxaloacetate; PPP, pentose phosphate pathway; Pyr, pyruvate; Succ, succinate; SuccCoA, succinyl-CoA; TCA, tricarboxylic acid cycle; αKG, α-ketoglutarate.

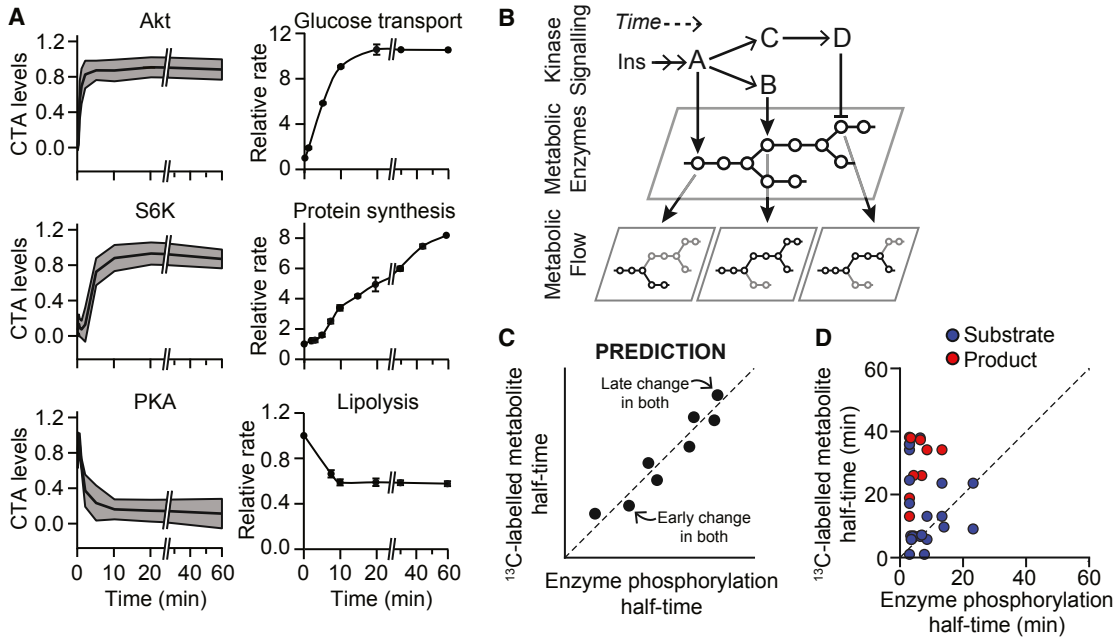

Figure 4. Kinase Activity Corresponds with Biological Processes but Precedes Changes in Glucose-Centric Metabolism

(A) 3T3-L1 adipocytes were serum starved and treated with insulin (100 nM) for varying time periods. Left: the activity (CTA) of each kinase was calculated based on the phosphorylation of the respective kinase's substrates. Data were sourced from Humphrey et al. (2013) and analyzed using the KSR-LIVE algorithm (Domanova et al., 2016). We extended our previous analysis of these data (Domanova et al., 2016) to include protein kinase A (PKA). Data were obtained from n = 3 biological samples per time point, presented as mean (solid black line) ± SD (gray shading). Right: glucose transport, protein synthesis, and lipolysis assays were performed as described in Experimental Procedures, and activity rates were made relative to the 0-min time point. Data are presented as mean ± SEM from at least n = 3 separate experiments for each activity assay.

(B) Hypothetical model. Details can be found in the Results.

(C and D) Enzymes were filtered for insulin-responsive phosphorylation sites and changes in ^{13}C-labeled levels of reactant metabolites, with substrates and products for each enzyme defined by KEGG (see Experimental Procedures for more details). For instance, phosphofructosekinase has fructose 6-phosphate as a substrate and fructose 1,6-bisphosphate as a product. For each enzyme, the half-times of changes in the ^{13}C-labeled levels of metabolites were plotted against the half-time of the earliest insulin-responsive phosphorylation site for that respective enzyme. The predicted result is a linear correlation whereby, for instance, a late phosphorylation event would be linked to a late change in metabolite levels (C). Actual result (D). For a significant majority of enzymes, the half-time of phosphorylation was smaller than that of the metabolites ($p < 0.001$ using binomial test).

glucose metabolism, with allosteric regulation being dominant, or that phosphorylation plays a more active role by priming the adipocyte to metabolize glucose via specific pathways. The latter is attractive as it suggests that protein phosphorylation plays a significant role in the selective changes in glucose metabolism in response to insulin (Figures 1E and 5).

Insulin-Stimulated Phosphorylation Primes the Adipocyte for Glucose Metabolism

We explored this further using glycogen synthesis as an example. Glycogen synthase (Gys) is activated by insulin signaling via rapid dephosphorylation of its inhibitory Ser-641 site (Figure 6A) (Rylatt et al., 1980; Skurat and Roach, 1995; Wang and Roach, 1993). This correlated well with its substrate, uridine diphosphate-glucose (UDP-Glc; Figure 6B); there was an initial drop in total UDP-Glc levels, with a steady state reached as (^{13}C-labeled) external glucose replenished this metabolite pool (Figure 6B). This pattern was not seen in the preceding metabolites (glucose 6-phosphate, glucose 1-phosphate), separating UDP-Glc by clustering (Figure 2D) and creating a negative crossover across the glycogen synthesis pathway (Figure S3A). This trend in UDP-Glc is unexpected, because if glycogen synthesis is predominantly driven by substrate accumulation (excess glucose) as previously reported (Bouskila et al., 2010), then total UDP-Glc levels should remain constant or increase (as one glucose molecule enters the UDP-Glc pool, one UDP-Glc molecule would be used for glycogen synthesis). This suggests glycogen synthesis in adipocytes is activated by insulin signaling before glucose transport is maximal.

To test whether glycogen synthesis is activated independently of glucose transport in the cell, we treated adipocytes with insulin alone, in the presence of an Akt inhibitor (MK2206), or in the absence of glucose. If the insulin response depends on glucose transport, then these perturbations should affect metabolites similarly (Figure 6C). We harvested polar metabolites and measured selected central carbon metabolites using a targeted liquid chromatography-coupled mass spectrometry (LC-MS) approach (Figure 6D). MK2206 and the absence of glucose both decreased most metabolites. However, these treatments had opposing effects on UDP-Glc (Figure 6D). UDP-Glc increased with MK2206, showing that insulin promotes UDP-Glc consumption via Akt, whereas UDP-Glc was consumed

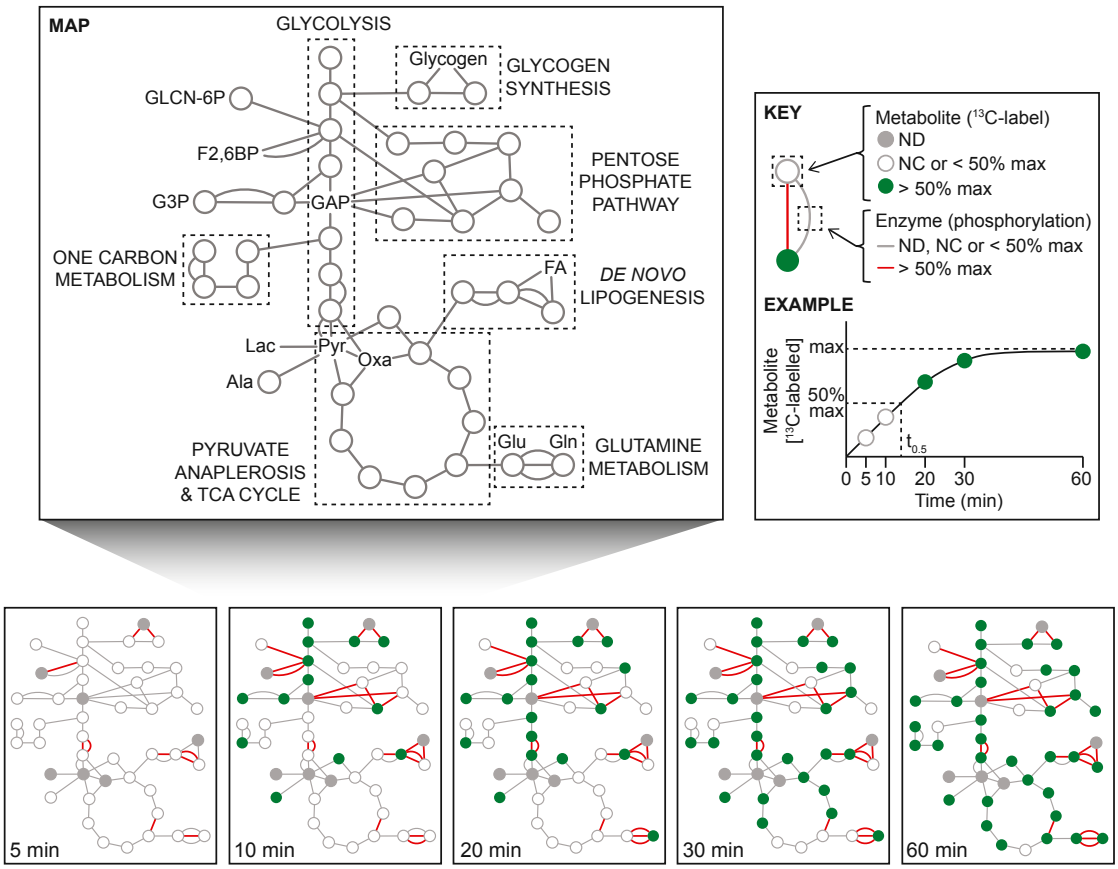

Figure 5. Overlaying Temporal Metabolomics and Phosphoproteomics Data Reveal that Insulin Stimulates the Phosphorylation of Metabolic Enzymes prior to Changes in Glucose-Centric Metabolism

Pathway representation of the insulin-responsive changes on the phosphoproteome and metabolome. Enzymes are depicted by lines and metabolites by dots. For each time point shown, metabolites whose ^{13}C-labeled levels had exceeded 50% of the maximum insulin-responsive change (increase/decrease) are depicted in green; an example is depicted in the key. Enzymes whose earliest insulin-responsive phosphorylation site exceeded 50% of the maximum change are depicted in red. Ala, alanine; F2,6BP, fructose 2,6-bisphosphate; FA, fatty acid; G3P, glycerol 3-phosphate; GAP, glyceraldehyde 3-phosphate; GLCN-6P, glucosamine 6-phosphate; Gln, glutamine; Glu, glutamate; Ins, insulin; Lac, lactate; NC, not changed. ND, not detected, measured or filtered out due to too many missing data points; Oxa, oxaloacetate; Pyr, pyruvate.

even in the absence of glucose (Figures 6D, S3B and S3C). This suggests that insulin can stimulate glycogen synthesis via Akt, independently of glucose uptake.

We complemented this by examining the incorporation of [U-^{14}C]-glucose into glycogen, a more direct measure of glycogen synthesis. Adipocytes were treated with insulin in the presence of a GLUT inhibitor cytochalasin B (CytoB; Figure 6C). This condition kept insulin signaling intact (Figure 6E) yet prevented insulin from significantly increasing glucose consumption (Figure 6F). In the presence of CytoB, insulin still stimulated ^{14}C-labeled glycogen production (Figure 6G). Consistent with our glucose-free treatment (Figure 6D), this suggests that insulin stimulated glucose incorporation into glycogen independently of glucose uptake.

DISCUSSION

Using dynamic ^{13}C-tracer metabolomics, we captured the acute metabolic response of adipocytes to insulin. There were rapid yet selective changes in the metabolome (Figures 1, 2, and 3). For instance, the upper and lower glycolysis were temporally segregated, with glucose metabolism observed only in specific branch points of glycolysis. Glucose transport accounted for a significant portion of the insulin-regulated metabolomic response. To explore how insulin may direct glucose metabolism beyond stimulating GLUT4-dependent glucose uptake, we integrated metabolomics and phosphoproteomics data. We observed that insulin-dependent phosphorylation of metabolic enzymes occurred rapidly and appeared to prime adipocytes for glucose metabolism (Figures 4, 5, and 6). These data unveil insight into an additional role for insulin action in the regulation of adipocyte glucose metabolism.

Recent steady-state fluxomics studies have yielded insights into adipocyte metabolism, including preferential substrates utilized for lipogenesis (Green et al., 2016) and sources of NADPH production (Liu et al., 2016). Our study presents a dynamic view of which metabolic features respond to insulin and on what timescale this occurs. For instance, the hexosamine pathway

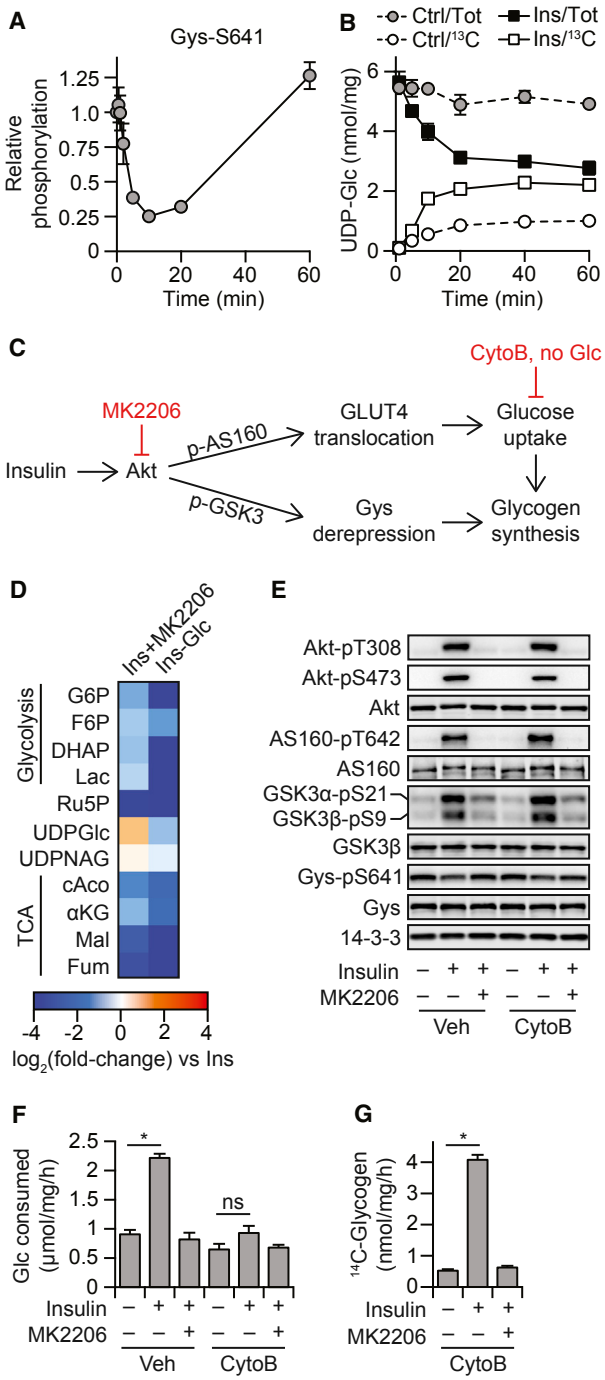

Figure 6. Insulin-Stimulated Phosphorylation Primes the Cell for Glucose Metabolism

3T3-L1 adipocytes were serum starved and treated with (Ins) or without (control [Ctrl]) 100 nM insulin for the indicated time points.

(A) Phosphorylation at residue Ser-641 of glycogen synthase (Gys) was measured using mass spectrometry. Data obtained from (Humphrey et al., 2013). Data are presented as mean ± SEM, relative to the 0-min time point, from n = 3 separate biological samples per time point.

(B) Total and ^{13}C-labeled levels of uridine diphosphate glucose (UDP-Glc) were measured as described in Figure 1A. Data presented as mean ± SEM from n = 3 separate experiments.

showed little change, while there was rapid accumulation of glycerol 3-phosphate (G3P) (Figure 1E). The latter may be due to GAPDH becoming rate limiting, based on the negative crossover at 2,3-diphosphoglycerate (Figure 1D), the lag in response between upper and lower glycolysis, and the large change in magnitude in fructose-1,6-bisphosphate levels (~10-fold at 10 min) (Figures 1D and 1E) (Shestov et al., 2014). This rise in G3P levels may help mediate the role of glucose in facilitating fatty acid storage into triglycerides (Beale et al., 2002; Reshef et al., 2003). Furthermore, temporal selectivity is seen within the PPP, with the oxidative PPP responding to insulin within minutes, whereas there was a late accumulation in phosphoribosyl pyrophosphate ($t_{1/2}$ >30 min), which connects the PPP to nucleotide metabolism. Together, this acute time course provides insight into which pathways are prioritized to achieve the general metabolic program of energy storage in the adipocyte.

Subsequently, this revealed metabolic priming by insulin signaling, which we propose plays a key role in regulating adipocyte metabolism. We used glycogen synthesis as an example (Figure 6), but there is evidence that this was a widespread phenomenon. For instance, a majority of TCA intermediates (citrate to succinate) initially decreased in total levels (Figure 3A). Citrate is also a substrate for the lipogenic enzyme ATP citrate lyase (ACLY), which was rapidly phosphorylated on an activating site (Ser-455) (Brownsey et al., 1984) in response to insulin (Figure S3D). Glucose subsequently replenished these TCA cycle intermediates. Thus, combined with fuelling oxidative PPP and pyruvate anaplerosis to provide NADPH (Figure 3A), glucose acted acutely at multiple nodes to support insulin-stimulated lipogenesis.

(C) Schematic depicting the treatments used in (D)–(G). Insulin activates Akt kinase, which phosphorylates AS160 (TBC1D4) to promote GLUT4 translocation and subsequent glucose uptake. Akt also phosphorylates GSK3 to derepress Gys. Combined, this stimulates glycogen synthesis. In (D)–(G), this is dissected by pharmacological inhibition of Akt (MK2206) or glucose uptake (CytoB or no glucose in the media).

(D) Following serum starvation, 3T3-L1 adipocytes were treated with insulin (Ins), Ins with 10 μM MK2206 (+MK2206), or Ins without glucose (−Glc), for 2 hr. Polar metabolites were analyzed by LC-MS, as described in the Experimental Procedures and the Supplemental Experimental Procedures. Changes in total levels of metabolites are presented as the mean fold-change compared to Ins-treated cells from n = 3 separate biological samples per condition.

(E) Following serum-starvation, 3T3-L1 adipocytes were treated with or without Ins, 10 μM MK2206, and 25 μM CytoB for 30 min. Cell lysates were subjected to western blotting and probed with the indicated antibodies. Blots are representative of n = 4 separate experiments.

(F and G) Following serum starvation, 3T3-L1 adipocytes were simultaneously radiolabelled with 1.5 μCi/mL [U-^{14}C]-glucose and treated with or without Ins, 10 μM MK2206, and 25 μM CytoB for 60 min. Media glucose levels were measured and media glucose consumption was calculated (F). *p < 0.05 (Student's t test); ns, no significant difference (Student's t test). Cells treated in the presence of CytoB were harvested for glycogen as described in the Experimental Procedures and the Supplemental Experimental Procedures (G). *p < 0.05 (Student's t test). Data are presented as mean ± SEM from n = 4 separate experiments.

cAco, *cis*-aconitate; DHAP, dihydroxyacetone phosphate; F6P, fructose 6-phosphate; Fum, fumarate; G6P, glucose 6-phosphate; Lac, lactate; Mal, malate; Ru5P, ribulose 5-phosphate; TCA, tricarboxylic acid; UDPGlc, uridine diphosphate glucose; UDPNAG, uridine diphosphate N-acetylglucosamine; Veh, vehicle; αKG, α-ketoglutarate.

Priming was also reflected in the dynamics of the energy charge ratio (Figure 3D). The initial decrease is consistent with an energy investment into anabolic pathways and the lag between upper (ATP investment) and lower (ATP production) glycolysis (Figures 1D and 1E). Overall, these data support a general notion that anabolic pathways are activated by insulin signaling, but this is done preemptively, before the accumulation of intracellular substrates. This initially depletes specific substrate pools, to pull the flow of glucose into anabolic pathways. This generates a demand-driven system, complementing the supply-driven regulation of anabolism by substrate accumulation, enabling insulin to prime the adipocyte for incoming glucose. This contrasts with β cell metabolism, where substrate availability governs glucose metabolism (Prentki et al., 2013).

This metabolic priming is a post-transcriptional example of "just-in-time" regulation (Zaslaver et al., 2004), a phenomenon observed in bacteria whereby optimal transcriptional regulation ensures only sufficient levels of enzymes are expressed with temporal precision to serve the cell's metabolic needs. It would be interesting to see whether priming applies to the catabolism of substrates other than glucose. For instance, there was a substantial unlabeled fraction of carbon in acetyl-coenzyme A (acetyl-CoA) (Figure 3A) (FC = 0.37 ± 0.02 at 60 min with insulin treatment), although pyruvate and its downstream metabolite, alanine, were mostly ^{13}C labeled (Figures S2B and S2C), suggesting the utilization of alternative carbon sources, such as amino acids (Green et al., 2016). Furthermore, it is tempting to speculate that disruption of insulin signaling to key metabolic priming events or insufficient glucose uptake to match the initial burst in anabolism may play a role in the cellular dysfunction associated with insulin resistance.

Together, this study highlights the benefit of comparing dynamics across multiple "omic" layers simultaneously. Using acute time points provided us with temporal resolution to identify the role of insulin-stimulated phosphorylation events beyond glucose transport. Such a transomic approach provides a more holistic view of cellular homeostasis, connecting physiological outputs to the underlying biological wiring (Yugi et al., 2016). Here, it has shed light on the orchestra of insulin signaling, which serves to complement metabolite-driven effects in the coordinated regulation of glucose metabolism. We envisage that future investigations will delineate the interplay between these forces in regulating metabolism through the development of new methods in quantifying non-steady-state flux and kinetic modeling.

EXPERIMENTAL PROCEDURES

For complete details, see Supplemental Experimental Procedures.

Dynamic Tracer Experiment

3T3-L1 adipocytes were serum-starved in serum-free DMEM (Sigma-Aldrich) containing 0.2% (w/v) BSA (Bovostar) and 2 mM GlutaMax (Life Technologies) for at least 1.5 hr. Cells were then labeled with ^{13}C-glucose and treated with or without 100 nM insulin for different lengths of time in a reverse time-course fashion (Figure 1A). This was performed in 6-well plates to ensure the wells could be harvested simultaneously at the end of the experiment. More specifically, following serum starvation each well was washed once with PBS and once with glucose-free DMEM (Sigma-Aldrich) and then incubated in glucose-free DMEM containing 0.2% (w/v) BSA, 1 mM GlutaMax, 1 mM glutamine (Life Technologies), and 25 mM [U-^{13}C]-labeled glucose (Omicron Biochemicals). This was identical to the serum-starvation media, except the glucose was now labeled and there was a more readily available source of glutamine. Cells were treated with or without 100 nM insulin at the time of media exchange. Following treatment, cell lysates were processed and analyzed by CE-MS or ion-chromatography-coupled mass spectrometry (MS).

Cell-Based Assays

3T3-L1 adipocytes were serum-starved prior to each experiment. In the single-time-point metabolomics experiment (Figure 6D), polar metabolites were analyzed by liquid chromatography-coupled tandem mass spectrometry (LC-MS/MS). To measure glucose transport, cells were incubated in Krebs-Ringer phosphate (KRP) buffer and treated with 100 nM insulin for different periods of time before being chilled on ice, exposed to ^{3}H-labeled 2-deoxyglucose (0.5 μCi/well; PerkinElmer) in 50 μM unlabeled 2-deoxyglucose for 5 min, and radioactivity was assessed in lysates by liquid scintillation counting. To measure protein synthesis, cells were incubated in leucine-free DMEM and treated with 100 nM insulin for different periods of time before being exposed to ^{3}H-labeled leucine (1.25 μCi/well; PerkinElmer) for 2 min and radioactivity assessed in the trichloroacetic acid-insoluble fractions of cell homogenates by liquid scintillation counting. To measure lipolysis, cells were incubated in KRP buffer supplemented with 3.5% fatty-acid free BSA, 5 mM glucose, and 5 μg/mL adenosine deaminase (all from Sigma-Aldrich). Cells were treated with insulin for different periods of time before being exposed to 1 nM isoproterenol in the last 7.5 min of insulin stimulation, and glycerol release was determined by media glycerol content using a glycerol assay kit (Sigma-Aldrich). To measure glucose consumption, media glucose content was determined using a glucose oxidase assay kit (Thermo Fisher Scientific). To measure glycogen synthesis, cells were labeled with ^{14}C-labeled glucose (PerkinElmer), quenched by freeze-thaw and lysed in 1 M KOH. Glycogen was precipitated using saturated Na_2SO_4 and ethanol and radioactivity determined by liquid scintillation counting. Data were normalized for protein content, which was measured using the BCA protein assay (Thermo Fisher Scientific).

Bioinformatics and Statistical Analyses

The raw metabolite data were used to calculate ^{13}C enrichments of metabolite backbone carbons, correcting for interference from the natural abundance of C, H, O, N, S, and P isotopes by using a least-square optimization approach in MATLAB R2015a (MathWorks, Natick MA).

To visualize the data by PCA, data preparation involved imputing missing metabolite concentrations for each time course by linear interpolation and normalization by log-transforming and subtracting the mean log concentration for each time course. The metabolite-domain PCA treated metabolomes at single time points as independent samples (n = 18), whereas the time-domain PCA treated single-metabolite time courses as independent samples (n = 134). This was performed using Python.

Metabolites whose total levels or FC changed in response to insulin were identified by comparing the area between the curves of the time courses of control and insulin-treated cells (Table S2; see Supplemental Experimental Procedures). Pathway enrichment analysis of changed metabolites was performed based on the Fisher exact test with Storey multiple test correction and pathways defined by the Kyoto Encyclopedia of Genes and Genomes (KEGG). The temporal patterns of metabolites were separated by comparing control and insulin-treated cells for each metabolite and subjecting the difference in total levels to hierarchical clustering and difference in maximum FC to the Otsu method for class separation. Half-times were calculated based on when each linearly interpolated time course crossed the midpoint between the initial value and maximum/minimum value; this was applied to the ^{13}C-labeled levels of metabolites and phosphorylation of metabolic enzymes. The latter was sourced from a previously published dataset (Humphrey et al., 2013), as described further in Supplemental Experimental Procedures. These analyses were performed using Python.

The figure legends provide details of additional statistical analyses, p value cutoffs, and the value and definition of "n" for each experiment.

SUPPLEMENTAL INFORMATION

Supplemental Information includes Supplemental Experimental Procedures, three figures, and three tables and can be found with this article online at https://doi.org/10.1016/j.celrep.2017.11.085.

ACKNOWLEDGMENTS

This work was supported by National Health and Medical Research Council (NHMRC) program grants (GNT1061122 and GNT1086850 to D.E.J.). J.R.K. and B.L.P. are recipients of NHMRC Early Career Fellowships (APP1072440 and APP1072129, respectively). D.E.J. is an NHMRC Senior Principal Research Fellow (APP1019680). S.K. was supported by the Creation of Fundamental Technologies for Understanding and Control of Biosystem Dynamics, CREST (JPMJCR12W3), from the Japan Science and Technology Agency (JST) and the Japan Society for the Promotion of Science (JSPS) (KAKENHI grant 17H06300). K.Y. was funded by the JSPS Grants-in-Aid for Scientific Research (KAKENHI grant JP15H05582) and by the Creation of Innovative Technology for Medical Applications Based on the Global Analyses and Regulation of Disease-Related Metabolites, PRESTO, from the JST. S.O. was funded by the JSPS (KAKENHI grant JP17K14864). A.H. was funded by the Research on Development of New Drugs (GAPFREE) from the Japan Agency for Medical Research and Development, AMED. T.S. was funded by the AMED-CREST from AMED. A.H. and T.S. were funded from Yamagata prefectural government and the City of Tsuruoka. L.-E.Q. was funded by the Judith and David Coffey Fund. Metabolomics Australia is part of the Bioplatforms Australia network, funded through the Australian Government's National Collaborative Research Infrastructure Strategy (NCRIS). The contents of the published material are solely the responsibility of the authors and do not reflect the views of the NHMRC.

AUTHOR CONTRIBUTIONS

Conceptualization, J.R.K., D.J.F., and D.E.J.; Investigation, J.R.K., D.J.F., A.H., M.P.H., B.L.P., M.E.N., S.I., F.S., and K.S.; Data curation, K.Y., L.-E.Q., J.R.K., and A.H.; Formal analysis, K.Y., R.S., and W.D.; Visualization, J.R.K., K.Y., and L.-E.Q.; Writing – Original Draft, J.R.K., K.Y., S.K., and D.E.J.; Writing –Review & Editing, J.R.K., K.Y., A.H., D.J.F., L.-E.Q., R.S., S.O., M.P.H., S.I., F.S., K.S., W.D., B.L.P., M.E.N., S.J.H., N.T., K.L.H., G.J.C., T.S., S.K., and D.E.J.; Resources, N.T., T.S., S.K., and D.E.J.; Funding acquisition, S.K. and D.E.J.; Supervision, S.K. and D.E.J.

DECLARATION OF INTERESTS

The authors declare no competing interests.

Received: August 17, 2017
Revised: September 6, 2017
Accepted: November 22, 2017
Published: December 19, 2017

REFERENCES

Abel, E.D., Peroni, O., Kim, J.K., Kim, Y.B., Boss, O., Hadro, E., Minnemann, T., Shulman, G.I., and Kahn, B.B. (2001). Adipose-selective targeting of the GLUT4 gene impairs insulin action in muscle and liver. Nature *409*, 729–733.

Atkinson, D.E. (1968). The energy charge of the adenylate pool as a regulatory parameter. Interaction with feedback modifiers. Biochemistry *7*, 4030–4034.

Beale, E.G., Hammer, R.E., Antoine, B., and Forest, C. (2002). Glyceroneogenesis comes of age. FASEB J. *16*, 1695–1696.

Bouskila, M., Hunter, R.W., Ibrahim, A.F., Delattre, L., Peggie, M., van Diepen, J.A., Voshol, P.J., Jensen, J., and Sakamoto, K. (2010). Allosteric regulation of glycogen synthase controls glycogen synthesis in muscle. Cell Metab. *12*, 456–466.

Brownsey, R.W., Edgell, N.J., Hopkirk, T.J., and Denton, R.M. (1984). Studies on insulin-stimulated phosphorylation of acetyl-CoA carboxylase, ATP citrate lyase and other proteins in rat epididymal adipose tissue. Evidence for activation of a cyclic AMP-independent protein kinase. Biochem. J. *218*, 733–743.

Bryant, N.J., Govers, R., and James, D.E. (2002). Regulated transport of the glucose transporter GLUT4. Nat. Rev. Mol. Cell Biol. *3*, 267–277.

Buescher, J.M., Antoniewicz, M.R., Boros, L.G., Burgess, S.C., Brunengraber, H., Clish, C.B., DeBerardinis, R.J., Feron, O., Frezza, C., Ghesquiere, B., et al. (2015). A roadmap for interpreting (13)C metabolite labeling patterns from cells. Curr. Opin. Biotechnol. *34*, 189–201.

DeFronzo, R.A., and Tripathy, D. (2009). Skeletal muscle insulin resistance is the primary defect in type 2 diabetes. Diabetes Care *32* (*Suppl 2*), S157–S163.

Domanova, W., Krycer, J., Chaudhuri, R., Yang, P., Vafaee, F., Fazakerley, D., Humphrey, S., James, D., and Kuncic, Z. (2016). Unraveling kinase activation dynamics using kinase-substrate relationships from temporal large-scale phosphoproteomics studies. PLoS ONE *11*, e0157763.

Foley, J.E., Foley, R., and Gliemann, J. (1980). Glucose-induced acceleration of deoxyglucose transport in rat adipocytes. Evidence for a second barrier to sugar entry. J. Biol. Chem. *255*, 9674–9677.

Garvey, W.T., and Kolterman, O.G. (1988). Correlation of in vivo and in vitro actions of insulin in obesity and noninsulin-dependent diabetes mellitus: role of the glucose transport system. Diabetes Metab. Rev. *4*, 543–569.

Green, C.R., Wallace, M., Divakaruni, A.S., Phillips, S.A., Murphy, A.N., Ciaraldi, T.P., and Metallo, C.M. (2016). Branched-chain amino acid catabolism fuels adipocyte differentiation and lipogenesis. Nat. Chem. Biol. *12*, 15–21.

Hackett, S.R., Zanotelli, V.R., Xu, W., Goya, J., Park, J.O., Perlman, D.H., Gibney, P.A., Botstein, D., Storey, J.D., and Rabinowitz, J.D. (2016). Systems-level analysis of mechanisms regulating yeast metabolic flux. Science *354*, aaf2786.

Herman, M.A., Peroni, O.D., Villoria, J., Schön, M.R., Abumrad, N.A., Blüher, M., Klein, S., and Kahn, B.B. (2012). A novel ChREBP isoform in adipose tissue regulates systemic glucose metabolism. Nature *484*, 333–338.

Holmes, W.F. (1959). Locating sites of interactions between external chemicals and a sequence of chemical reactions. Trans. Faraday Soc. *55*, 1122–1126.

Humphrey, S.J., Yang, G., Yang, P., Fazakerley, D.J., Stöckli, J., Yang, J.Y., and James, D.E. (2013). Dynamic adipocyte phosphoproteome reveals that Akt directly regulates mTORC2. Cell Metab. *17*, 1009–1020.

Katz, J., and Rognstad, R. (1966). The metabolism of tritiated glucose by rat adipose tissue. J. Biol. Chem. *241*, 3600–3610.

Katz, J., Landau, B.R., and Bartsch, G.E. (1966). The pentose cycle, triose phosphate isomerization, and lipogenesis in rat adipose tissue. J. Biol. Chem. *241*, 727–740.

Kraegen, E.W., Clark, P.W., Jenkins, A.B., Daley, E.A., Chisholm, D.J., and Storlien, L.H. (1991). Development of muscle insulin resistance after liver insulin resistance in high-fat-fed rats. Diabetes *40*, 1397–1403.

Liu, L., Shah, S., Fan, J., Park, J.O., Wellen, K.E., and Rabinowitz, J.D. (2016). Malic enzyme tracers reveal hypoxia-induced switch in adipocyte NADPH pathway usage. Nat. Chem. Biol. *12*, 345–352.

Marshall, S. (1989). Kinetics of insulin action on protein synthesis in isolated adipocytes. Ability of glucose to selectively desensitize the glucose transport system without altering insulin stimulation of protein synthesis. J. Biol. Chem. *264*, 2029–2036.

McGarry, J.D., Takabayashi, Y., and Foster, D.W. (1978). The role of malonyl-coa in the coordination of fatty acid synthesis and oxidation in isolated rat hepatocytes. J. Biol. Chem. *253*, 8294–8300.

Moreno-Sánchez, R., Saavedra, E., Rodríguez-Enríquez, S., and Olín-Sandoval, V. (2008). Metabolic control analysis: a tool for designing strategies to manipulate metabolic pathways. J. Biomed. Biotechnol. *2008*, 597913.

Prentki, M., Matschinsky, F.M., and Madiraju, S.R. (2013). Metabolic signaling in fuel-induced insulin secretion. Cell Metab. *18*, 162–185.

Reshef, L., Olswang, Y., Cassuto, H., Blum, B., Croniger, C.M., Kalhan, S.C., Tilghman, S.M., and Hanson, R.W. (2003). Glyceroneogenesis and the triglyceride/fatty acid cycle. J. Biol. Chem. *278*, 30413–30416.

Rodbell, M. (1964). Metabolism of isolated fat cells. I. Effects of hormones on glucose metabolism and lipolysis. J. Biol. Chem. *239*, 375–380.

Rosen, E.D., and Spiegelman, B.M. (2014). What we talk about when we talk about fat. Cell *156*, 20–44.

Rylatt, D.B., Aitken, A., Bilham, T., Condon, G.D., Embi, N., and Cohen, P. (1980). Glycogen synthase from rabbit skeletal muscle. Amino acid sequence at the sites phosphorylated by glycogen synthase kinase-3, and extension of the N-terminal sequence containing the site phosphorylated by phosphorylase kinase. Eur. J. Biochem. *107*, 529–537.

Shestov, A.A., Liu, X., Ser, Z., Cluntun, A.A., Hung, Y.P., Huang, L., Kim, D., Le, A., Yellen, G., Albeck, J.G., and Locasale, J.W. (2014). Quantitative determinants of aerobic glycolysis identify flux through the enzyme GAPDH as a limiting step. eLife *3*, e03342.

Skurat, A.V., and Roach, P.J. (1995). Phosphorylation of sites 3a and 3b (Ser640 and Ser644) in the control of rabbit muscle glycogen synthase. J. Biol. Chem. *270*, 12491–12497.

Stöckli, J., Fazakerley, D.J., and James, D.E. (2011). GLUT4 exocytosis. J. Cell Sci. *124*, 4147–4159.

Turner, N., Kowalski, G.M., Leslie, S.J., Risis, S., Yang, C., Lee-Young, R.S., Babb, J.R., Meikle, P.J., Lancaster, G.I., Henstridge, D.C., et al. (2013). Distinct patterns of tissue-specific lipid accumulation during the induction of insulin resistance in mice by high-fat feeding. Diabetologia *56*, 1638–1648.

Wang, Y., and Roach, P.J. (1993). Inactivation of rabbit muscle glycogen synthase by glycogen synthase kinase-3. Dominant role of the phosphorylation of Ser-640 (site-3a). J. Biol. Chem. *268*, 23876–23880.

Winegrad, A.I., and Renold, A.E. (1958a). Studies on rat adipose tissue in vitro. I. Effects of insulin on the metabolism of glucose, pyruvate, and acetate. J. Biol. Chem. *233*, 267–272.

Winegrad, A.I., and Renold, A.E. (1958b). Studies on rat adipose tissue in vitro. II. Effects of insulin on the metabolism of specifically labeled glucose. J. Biol. Chem. *233*, 273–276.

Yugi, K., Kubota, H., Toyoshima, Y., Noguchi, R., Kawata, K., Komori, Y., Uda, S., Kunida, K., Tomizawa, Y., Funato, Y., et al. (2014). Reconstruction of insulin signal flow from phosphoproteome and metabolome data. Cell Rep. *8*, 1171–1183.

Yugi, K., Kubota, H., Hatano, A., and Kuroda, S. (2016). Trans-omics: how to reconstruct biochemical networks across multiple 'omic' layers. Trends Biotechnol. *34*, 276–290.

Zaslaver, A., Mayo, A.E., Rosenberg, R., Bashkin, P., Sberro, H., Tsalyuk, M., Surette, M.G., and Alon, U. (2004). Just-in-time transcription program in metabolic pathways. Nat. Genet. *36*, 486–491.